5-1-2022

Search for High-energy Neutrino Emission from Galactic X-Ray Binaries with IceCube

R. Abbasi
Loyola University of Chicago

M. Ackermann
Deutsches Elektronen-Synchrotron (DESY)

J. Adams
University of Canterbury

J. A. Aguilar
Université Libre de Bruxelles

M. Ahlers
Niels Bohr Institutet

See next page for additional authors

The Astrophysical Journal Letters, 930:L24 (13pp), 2022 May 10 https://doi.org/10.3847/2041-8213/ac67d8

Search for High-energy Neutrino Emission from Galactic X-Ray Binaries with IceCube

R. Abbasi[1], M. Ackermann[2], J. Adams[3], J. A. Aguilar[4], M. Ahlers[5], M. Ahrens[6], J. M. Alameddine[7], A. A. Alves, Jr.[8], N. M. Amin[9], K. Andeen[10], T. Anderson[11], G. Anton[12], C. Argüelles[13], Y. Ashida[14], S. Axani[15], X. Bai[16], A. Balagopal V.[14], S. W. Barwick[17], B. Bastian[2], V. Basu[14], S. Baur[4], R. Bay[18], J. J. Beatty[19,20], K.-H. Becker[21], J. Becker Tjus[22], J. Beise[23], C. Bellenghi[24], S. Benda[14], S. BenZvi[25], D. Berley[26], E. Bernardini[2,62], D. Z. Besson[27], G. Binder[18,28], D. Bindig[21], E. Blaufuss[26], S. Blot[2], M. Boddenberg[29], F. Bontempo[8], J. Borowka[29], S. Böser[30], O. Botner[23], J. Böttcher[29], E. Bourbeau[5], F. Bradascio[2], J. Braun[14], B. Brinson[31], S. Bron[32], J. Brostean-Kaiser[2], S. Browne[33], A. Burgman[23], R. T. Burley[34], R. S. Busse[35], M. A. Campana[36], E. G. Carnie-Bronca[34], C. Chen[31], Z. Chen[37], D. Chirkin[14], K. Choi[38], B. A. Clark[39], K. Clark[40], L. Classen[35], A. Coleman[9], G. H. Collin[15], J. M. Conrad[15], P. Coppin[41], P. Correa[41], D. F. Cowen[11,42], R. Cross[25], C. Dappen[29], P. Dave[31], C. De Clercq[41], J. J. DeLaunay[43], D. Delgado López[13], H. Dembinski[9], K. Deoskar[6], A. Desai[14], P. Desiati[14], K. D. de Vries[41], G. de Wasseige[44], M. de With[45], T. DeYoung[39], A. Diaz[15], J. C. Díaz-Vélez[14], M. Dittmer[35], H. Dujmovic[8], M. Dunkman[11], M. A. DuVernois[14], T. Ehrhardt[30], P. Eller[24], R. Engel[8,33], H. Erpenbeck[29], J. Evans[26], P. A. Evenson[9], K. L. Fan[26], A. R. Fazely[46], A. Fedynitch[47], N. Feigl[45], S. Fiedlschuster[12], A. T. Fienberg[11], C. Finley[6], L. Fischer[2], D. Fox[42], A. Franckowiak[2,22], E. Friedman[26], A. Fritz[30], P. Fürst[29], T. K. Gaisser[9], J. Gallagher[48], E. Ganster[29], A. Garcia[13], S. Garrappa[2], L. Gerhardt[28], A. Ghadimi[43], C. Glaser[23], T. Glauch[24], T. Glüsenkamp[12], J. G. Gonzalez[9], S. Goswami[43], D. Grant[39], T. Grégoire[11], S. Griswold[25], C. Günther[29], P. Gutjahr[7], C. Haack[24], A. Hallgren[23], R. Halliday[39], L. Halve[29], F. Halzen[14], M. Ha Minh[24], K. Hanson[14], J. Hardin[14], A. A. Harnisch[39], A. Haungs[8], D. Hebecker[45], K. Helbing[21], F. Henningsen[24], E. C. Hettinger[39], S. Hickford[21], J. Hignight[49], C. Hill[50], G. C. Hill[34], K. D. Hoffman[26], R. Hoffmann[21], K. Hoshina[14,63], F. Huang[11], M. Huber[24], T. Huber[8], K. Hultqvist[6], M. Hünnefeld[7], R. Hussain[14], K. Hymon[7], S. In[38], N. Iovine[4], A. Ishihara[50], M. Jansson[6], G. S. Japaridze[51], M. Jeong[38], M. Jin[13], B. J. P. Jones[52], D. Kang[8], W. Kang[38], X. Kang[36], A. Kappes[35], D. Kappesser[30], L. Kardum[7], T. Karg[2], M. Karl[24], A. Karle[14], U. Katz[12], M. Kauer[14], M. Kellermann[29], J. L. Kelley[14], A. Kheirandish[11], K. Kin[50], T. Kintscher[2], J. Kiryluk[37], S. R. Klein[18,28], A. Kochocki[39], R. Koirala[9], H. Kolanoski[45], T. Kontrimas[24], L. Köpke[30], C. Kopper[39], S. Kopper[43], D. J. Koskinen[5], P. Koundal[8], M. Kovacevich[36], M. Kowalski[2,45], T. Kozynets[5], E. Krupczak[39], E. Kun[22], N. Kurahashi[36], N. Lad[2], C. Lagunas Gualda[2], J. L. Lanfranchi[11], M. J. Larson[26], F. Lauber[21], J. P. Lazar[13,14], J. W. Lee[38], K. Leonard[14], A. Leszczyńska[33], Y. Li[11], M. Lincetto[22], Q. R. Liu[14], M. Liubarska[49], E. Lohfink[30], C. J. Lozano Mariscal[35], L. Lu[14], F. Lucarelli[32], A. Ludwig[39,53], W. Luszczak[14], Y. Lyu[18,28], W. Y. Ma[2], J. Madsen[14], K. B. M. Mahn[39], Y. Makino[14], S. Mancina[14], I. C. Mariş[4], I. Martinez-Soler[13], R. Maruyama[54], S. McCarthy[14], T. McElroy[49], F. McNally[55], J. V. Mead[5], K. Meagher[14], S. Mechbal[2], A. Medina[20], M. Meier[50], S. Meighen-Berger[24], J. Micallef[39], D. Mockler[4], T. Montaruli[32], R. W. Moore[49], R. Morse[14], M. Moulai[15], R. Naab[2], R. Nagai[50], U. Naumann[21], J. Necker[2], L. V. Nguyễn[39], H. Niederhausen[39], M. U. Nisa[39], S. C. Nowicki[39], A. Obertacke Pollmann[21], M. Oehler[8], B. Oeyen[56], A. Olivas[26], E. O'Sullivan[23], H. Pandya[9], D. V. Pankova[11], N. Park[40], G. K. Parker[52], E. N. Paudel[9], L. Paul[10], C. Pérez de los Heros[23], L. Peters[29], J. Peterson[14], S. Philippen[29], S. Pieper[21], M. Pittermann[33], A. Pizzuto[14], M. Plum[16], Y. Popovych[30], A. Porcelli[56], M. Prado Rodriguez[14], B. Pries[39], G. T. Przybylski[28], C. Raab[4], J. Rack-Helleis[30], A. Raissi[3], M. Rameez[5], K. Rawlins[57], I. C. Rea[24], Z. Rechav[14], A. Rehman[9], P. Reichherzer[22], R. Reimann[29], G. Renzi[4], E. Resconi[24], S. Reusch[2], W. Rhode[7], M. Richman[36], B. Riedel[14], E. J. Roberts[34], S. Robertson[18,28], G. Roellinghoff[38], M. Rongen[30], C. Rott[38,58], T. Ruhe[7], D. Ryckbosch[56], D. Rysewyk Cantu[39], I. Safa[13,14], J. Saffer[33], S. E. Sanchez Herrera[39], A. Sandrock[7], M. Santander[43], S. Sarkar[59], S. Sarkar[49], K. Satalecka[2], M. Schaufel[29], H. Schieler[8], S. Schindler[12], T. Schmidt[26], A. Schneider[14], J. Schneider[12], F. G. Schröder[8,9], L. Schumacher[24], G. Schwefer[29], S. Sclafani[36], D. Seckel[9], S. Seunarine[60], A. Sharma[23], S. Shefali[33], N. Shimizu[50], M. Silva[14], B. Skrzypek[13], B. Smithers[52], R. Snihur[14], J. Soedingrekso[7], D. Soldin[9], C. Spannfellner[24], G. M. Spiczak[60], C. Spiering[2], J. Stachurska[2], M. Stamatikos[20], T. Stanev[9], R. Stein[2], J. Stettner[29], T. Stezelberger[28], T. Stürwald[21], T. Stuttard[5], G. W. Sullivan[26], I. Taboada[31], S. Ter-Antonyan[46], J. Thwaites[14], S. Tilav[9], F. Tischbein[29], K. Tollefson[39], C. Tönnis[61], S. Toscano[4], D. Tosi[14], A. Trettin[2], M. Tselengidou[12], C. F. Tung[31], A. Turcati[24], R. Turcotte[8], C. F. Turley[11], J. P. Twagirayezu[39], B. Ty[14], M. A. Unland Elorrieta[35], N. Valtonen-Mattila[23], J. Vandenbroucke[14], N. van Eijndhoven[41], D. Vannerom[15], J. van Santen[2], J. Veitch-Michaelis[14], S. Verpoest[56], C. Walck[6], W. Wang[14], T. B. Watson[52], C. Weaver[39], P. Weigel[15], A. Weindl[8], M. J. Weiss[11], J. Weldert[30], C. Wendt[14], J. Werthebach[7], M. Weyrauch[33], N. Whitehorn[39,53], C. H. Wiebusch[29], N. Willey[39], D. R. Williams[43], M. Wolf[14], G. Wrede[12], J. Wulff[22], X. W. Xu[46], J. P. Yanez[49], E. Yildizci[14], S. Yoshida[50], S. Yu[39], T. Yuan[14], Z. Zhang[37], and P. Zhelnin[13]

[1] Department of Physics, Loyola University Chicago, Chicago, IL 60660, USA; analysis@icecube.wisc.edu
[2] DESY, D-15738 Zeuthen, Germany
[3] Department of Physics and Astronomy, University of Canterbury, Private Bag 4800, Christchurch, New Zealand
[4] Université Libre de Bruxelles, Science Faculty CP230, B-1050 Brussels, Belgium
[5] Niels Bohr Institute, University of Copenhagen, DK-2100 Copenhagen, Denmark
[6] Oskar Klein Centre and Dept. of Physics, Stockholm University, SE-10691 Stockholm, Sweden

[7] Dept. of Physics, TU Dortmund University, D-44221 Dortmund, Germany
[8] Karlsruhe Institute of Technology, Institute for Astroparticle Physics, D-76021 Karlsruhe, Germany
[9] Bartol Research Institute and Dept. of Physics and Astronomy, University of Delaware, Newark, DE 19716, USA
[10] Department of Physics, Marquette University, Milwaukee, WI 53201, USA
[11] Dept. of Physics, Pennsylvania State University, University Park, PA 16802, USA
[12] Erlangen Centre for Astroparticle Physics, Friedrich-Alexander-Universität Erlangen-Nürnberg, D-91058 Erlangen, Germany
[13] Department of Physics and Laboratory for Particle Physics and Cosmology, Harvard University, Cambridge, MA 02138, USA
[14] Dept. of Physics and Wisconsin IceCube Particle Astrophysics Center, University of Wisconsin–Madison, Madison, WI 53706, USA
[15] Dept. of Physics, Massachusetts Institute of Technology, Cambridge, MA 02139, USA
[16] Physics Department, South Dakota School of Mines and Technology, Rapid City, SD 57701, USA
[17] Dept. of Physics and Astronomy, University of California, Irvine, CA 92697, USA
[18] Dept. of Physics, University of California, Berkeley, CA 94720, USA
[19] Dept. of Astronomy, Ohio State University, Columbus, OH 43210, USA
[20] Dept. of Physics and Center for Cosmology and Astro-Particle Physics, Ohio State University, Columbus, OH 43210, USA
[21] Dept. of Physics, University of Wuppertal, D-42119 Wuppertal, Germany
[22] Fakultät für Physik & Astronomie, Ruhr-Universität Bochum, D-44780 Bochum, Germany
[23] Dept. of Physics and Astronomy, Uppsala University, Box 516, SE-75120 Uppsala, Sweden
[24] Physik-department, Technische Universität München, D-85748 Garching, Germany
[25] Dept. of Physics and Astronomy, University of Rochester, Rochester, NY 14627, USA
[26] Dept. of Physics, University of Maryland, College Park, MD 20742, USA
[27] Dept. of Physics and Astronomy, University of Kansas, Lawrence, KS 66045, USA
[28] Lawrence Berkeley National Laboratory, Berkeley, CA 94720, USA
[29] III. Physikalisches Institut, RWTH Aachen University, D-52056 Aachen, Germany
[30] Institute of Physics, University of Mainz, Staudinger Weg 7, D-55099 Mainz, Germany
[31] School of Physics and Center for Relativistic Astrophysics, Georgia Institute of Technology, Atlanta, GA 30332, USA
[32] Département de physique nucléaire et corpusculaire, Université de Genève, CH-1211 Genève, Switzerland
[33] Karlsruhe Institute of Technology, Institute of Experimental Particle Physics, D-76021 Karlsruhe, Germany
[34] Department of Physics, University of Adelaide, Adelaide, 5005, Australia
[35] Institut für Kernphysik, Westfälische Wilhelms-Universität Münster, D-48149 Münster, Germany
[36] Dept. of Physics, Drexel University, 3141 Chestnut Street, Philadelphia, PA 19104, USA
[37] Dept. of Physics and Astronomy, Stony Brook University, Stony Brook, NY 11794-3800, USA
[38] Dept. of Physics, Sungkyunkwan University, Suwon 16419, Republic of Korea
[39] Dept. of Physics and Astronomy, Michigan State University, East Lansing, MI 48824, USA
[40] Dept. of Physics, Engineering Physics, and Astronomy, Queen's University, Kingston, ON K7L 3N6, Canada
[41] Vrije Universiteit Brussel (VUB), Dienst ELEM, B-1050 Brussels, Belgium
[42] Dept. of Astronomy and Astrophysics, Pennsylvania State University, University Park, PA 16802, USA
[43] Dept. of Physics and Astronomy, University of Alabama, Tuscaloosa, AL 35487, USA
[44] Centre for Cosmology, Particle Physics and Phenomenology—CP3, Université catholique de Louvain, Louvain-la-Neuve, Belgium
[45] Institut für Physik, Humboldt-Universität zu Berlin, D-12489 Berlin, Germany
[46] Dept. of Physics, Southern University, Baton Rouge, LA 70813, USA
[47] Institute of Physics, Academia Sinica, Taipei, 11529, Taiwan
[48] Dept. of Astronomy, University of Wisconsin–Madison, Madison, WI 53706, USA
[49] Dept. of Physics, University of Alberta, Edmonton, Alberta, T6G 2E1, Canada
[50] Dept. of Physics and The International Center for Hadron Astrophysics, Chiba University, Chiba 263-8522, Japan
[51] CTSPS, Clark-Atlanta University, Atlanta, GA 30314, USA
[52] Dept. of Physics, University of Texas at Arlington, 502 Yates St., Science Hall Rm 108, Box 19059, Arlington, TX 76019, USA
[53] Department of Physics and Astronomy, UCLA, Los Angeles, CA 90095, USA
[54] Dept. of Physics, Yale University, New Haven, CT 06520, USA
[55] Department of Physics, Mercer University, Macon, GA 31207-0001, USA
[56] Dept. of Physics and Astronomy, University of Gent, B-9000 Gent, Belgium
[57] Dept. of Physics and Astronomy, University of Alaska Anchorage, 3211 Providence Dr., Anchorage, AK 99508, USA
[58] Department of Physics and Astronomy, University of Utah, Salt Lake City, UT 84112, USA
[59] Dept. of Physics, University of Oxford, Parks Road, Oxford OX1 3PU, UK
[60] Dept. of Physics, University of Wisconsin, River Falls, WI 54022, USA
[61] Institute of Basic Science, Sungkyunkwan University, Suwon 16419, Republic of Korea
Received 2022 March 1; revised 2022 April 11; accepted 2022 April 16; published 2022 May 16

Abstract

We present the first comprehensive search for high-energy neutrino emission from high- and low-mass X-ray binaries conducted by IceCube. Galactic X-ray binaries are long-standing candidates for the source of Galactic hadronic cosmic rays and neutrinos. The compact object in these systems can be the site of cosmic-ray acceleration, and neutrinos can be produced by interactions of cosmic rays with radiation or gas, in the jet of a microquasar, in the stellar wind, or in the atmosphere of the companion star. We study X-ray binaries using 7.5 yr of IceCube data with three separate analyses. In the first, we search for periodic neutrino emission from 55 binaries

[62] Also at Università di Padova, I-35131 Padova, Italy.
[63] Also at Earthquake Research Institute, University of Tokyo, Bunkyo, Tokyo 113-0032, Japan.

in the Northern Sky with known orbital periods. In the second, the X-ray light curves of 102 binaries across the entire sky are used as templates to search for time-dependent neutrino emission. Finally, we search for time-integrated emission of neutrinos for a list of 4 notable binaries identified as microquasars. In the absence of a significant excess, we place upper limits on the neutrino flux for each hypothesis and compare our results with theoretical predictions for several binaries. In addition, we evaluate the sensitivity of the next generation neutrino telescope at the South Pole, IceCube-Gen2, and demonstrate its power to identify potential neutrino emission from these binary sources in the Galaxy.

Unified Astronomy Thesaurus concepts: Neutrino astronomy (1100); Neutrino telescopes (1105); X-ray binary stars (1811); Galactic cosmic rays (567)

1. Introduction

Cosmic rays (CRs) up to several PeV, the "knee" in the CR spectrum, are believed to be of Galactic origin. However, where and how these CRs are accelerated remains an open question. Interactions of hadronic CRs in the Galaxy will lead to the production of pions, which subsequently decay into gamma-rays and neutrinos with energies potentially reaching hundreds of TeV. Unlike gamma-rays which could also be produced by accelerated electrons/positrons, high-energy neutrinos would be the smoking-gun for CR interactions as they are the only way to produce neutrinos. In 2013, IceCube discovered TeV–PeV neutrinos of astrophysical origin (Aartsen et al. 2013a, 2014). Nevertheless, the sources of those high-energy neutrinos are yet to be identified. Since the discovery of high-energy cosmic neutrinos by IceCube, many studies have been conducted searching for neutrino emission from point-like sources, extended regions, and the diffuse emission from CRs interacting with the Galactic interstellar medium. The isotropic distribution of neutrino events in IceCube suggests a dominant contribution from extragalactic sources and constrains the Galactic contribution to the diffuse neutrino flux to less than 14% above 1 TeV (Aartsen et al. 2017a).

Recent searches for correlations with Galactic sources show no evidence of a signal (e.g., Albert et al. 2018, Kheirandish & Wood 2020, Aartsen et al. 2020a) and so far, only a blazar, TXS 0506+056, which is extragalactic, shows evidence of being a neutrino source (Aartsen et al. 2018a, 2018b).

X-ray binaries (XRBs) are binary systems that emit X-rays and consist of a compact object (neutron star (NS) or black hole (BH)) and a non-compact companion star. The mass from the companion is accreted onto the compact object due to the strong gravitational attraction forming an accretion disk. Depending on the mass of the companion star, XRBs can be divided into high-mass XRBs (HMXBs) and low-mass XRBs (LMXBs). The companion star of an HMXB is massive, usually an O or B-type star, and the accretion is mainly a result of stellar wind capture (Liu et al. 2006). LMXBs have companion stars of A-type or later, and the mass transfer is mostly caused by Roche lobe overflows (Liu et al. 2007). These systems are bright in X-rays and sometimes in gamma-rays. XRBs have been proposed as sites of CR acceleration and hadronic interactions since the 1980s (e.g., Berezinsky et al. 1985; Gaisser & Stanev 1985). Microquasars, which are XRBs with relativistic jets (Mirabel et al. 1992), are miniature analogs of quasars, a category of extremely luminous active galactic nuclei. It is expected that the similarity may not only be morphological, but also in the physics of the formation of the accretion disk and the behavior of the jet, at different luminosity scales. Hadronic processes in jets of microquasars have been widely discussed. Protons can be accelerated in the jet, and pions are generated through interactions with the external radiation field of the accretion disk and/or internal synchrotron photons ($p\gamma$) (Levinson & Waxman 2001; Distefano et al. 2002; Romero & Vila 2008). Other scenarios focus on hadronuclear interactions (pp), e.g., jet-cloud/wind interactions when the jet traversing the matter field of the ejected clouds or stellar wind from the companion star (Aharonian & Atoyan 1991; Romero et al. 2003; Bednarek 2005). For other XRBs without collimated beams, hadronic interactions happen in a wider shocked region. CR can be accelerated in the magnetosphere of a spinning NS and then interact with matter from either the accretion disk or the companion star (Berezinsky et al. 1985; Gaisser & Stanev 1985; Kolb et al. 1985; Cheng & Ruderman 1989; Anchordoqui et al. 2003).

Some XRBs have been observed in TeV gamma-rays, which may suggest acceleration of hadrons besides an origin of accelerated leptons. Neutrino production in those sources and the potential of IceCube detection have been discussed, e.g., LS 5039 (Aharonian et al. 2006), LS I+61 303 (Christiansen et al. 2006; Torres & Halzen 2007), and SS 433 (Reynoso & Carulli 2019; Kimura et al. 2020).

XRBs exhibit both outbursts and periodic emissions. It is reasonable to hypothesize that the possible neutrino emission is related to either the periodicity or the X-ray outbursts. Conducting time-dependent studies incorporating these hypotheses provides the advantage of suppressing background. Both time-integrated and time-dependent analyses searching for neutrino emission from the entire sky have been performed by IceCube (Abbasi et al. 2012; Aartsen et al. 2013b, 2014, 2015) and ANTARES (Adrian-Martinez et al. 2014; Albert et al. 2017) previously, without significant signal detection. Here, we present a comprehensive high-energy neutrino search focusing on XRBs using 7.5 yr of IceCube data. This study explores the periodic, X-ray outburst-correlated, and persistent emission scenarios of the possible neutrino flux from XRBs, while covering a broader list of sources compared to previous studies.

2. Detector and Data Set

The IceCube Neutrino Observatory, built under the ice surface at the South Pole, is a 1 km^3 Cherenkov neutrino telescope. The detector is composed of an array of digital optical modules (DOMs), each equipped with a photomultiplier tube (PMT) and on-board read-out electronics. The PMTs in the DOMs collect the Cherenkov photons emitted by the relativistic charged particles produced in neutrino interactions when traversing the ice. The number of detected photons and their arrival time information are used to reconstruct the energy and direction of each event. Different neutrino flavors and interactions can result in different event signatures inside IceCube detection volume. Among them, muon tracks from $\nu_\mu/\bar{\nu}_\mu$ charged-current interactions can be reconstructed with a good angular resolution, typically $\lesssim 1^\circ$ (Aartsen et al. 2017b), which makes them ideal for neutrino point source searches.

Table 1
Table of the Most Significant Sources

Analysis	Source	TS	$\hat{n}_s$	$\hat{\gamma}$	p-value
Periodic	V635 Cas	9.07	50.5	4	0.25 (0.0052)
Flare	V404 Cyg	8.28	5.4	4	0.75 (0.014)
Time-integrated	Cyg X-3	6.81	44.6	3.25	0.036 (0.009)

Note. The most significant source in each analysis with its best-fitted TS, $\hat{n}_s$, $\hat{\gamma}$. Both post-trial and pre-trial (bracketed) p-values are shown. The trial correction is calculated by considering the number of sources studied in each analysis respectively and has a relation $p_{\rm post} = 1 - (1 - p_{\rm pre})^N$, where N is the source number.

In this search, we use 7.5 yr of all-sky muon track data collected between 2011 May 13 and 2018 October 14, with an effective livetime of 2711 days. The data sample being used has an event selection focusing on high-quality through-going neutrino track events from the entire sky with an energy threshold near 100 GeV. The final event rate is ∼6 mHz, yielding a total of 1,502,612 events. A better sensitivity in the Northern Hemisphere is expected due to the suppression of the atmospheric muon background by Earth for up-going events. Details of the data sample are described in Aartsen et al. (2017c).

3. Analysis

The three analyses use an unbinned maximum likelihood-ratio method (Braun et al. 2008, 2010) to search for an excess of neutrino events above the background of atmospheric muon, atmospheric and isotropic astrophysical neutrino flux in the direction of selected XRBs. In all analyses, the likelihood function describing the signal includes both a directional correlation and an energy spectrum assumed to follow a power law, i.e., $\propto E^{-\gamma}$. For the time-dependent analyses, each incorporates a unique temporal term in the likelihood to model the signal. As the data is expected to be background-dominated, which is uniform in time, the background probability density function (PDF) is constructed from time-randomized data. The test statistic (TS) is obtained by maximizing the likelihood ratio with respect to a set of parameters, which includes the number of signal events (n_s) and a power-law spectral index (γ). Other parameters are analysis-specific, e.g., time of the neutrino emission and the duration. A more detailed description of the method can be found in the Appendix A. The sources studied are from a catalog of 114 Galactic HMXBs (Liu et al. 2006) and 187 LMXBs (Liu et al. 2007). Furthermore, we added 7 TeV XRBs from TeVCat[64] very-high-energy gamma-ray catalog (Wakely & Horan 2008), which are not in the HMXB or LMXB catalog. Additional selection criteria are then applied to this initial source list in the two time-dependent analyses (as explained in Sections 3.1 and 3.2), leading to two different source lists with an overlap. We also include a time-integrated search on four individual sources. The rest of this section includes the description of each analysis and its results. Table 1 summarizes the most statistically significant source in each analysis.

3.1. Periodic Analysis

Periodic searches have been previously performed by IceCube using data of 2007–2009 with a partially built configuration and 2008–2012, including the first year of the completed detector (Abbasi et al. 2012; Aartsen et al. 2015), assuming that the neutrino emission from XRBs is modulated by orbital periods. In the period-folded phase space, these neutrinos should appear as at the same phase. As an improvement on prior work, the temporal signal PDF in the phase space is modeled by a von Mises distribution instead of a Gaussian distribution (see Appendix A.1). The choice of the von Mises distribution is to satisfy the periodic boundary condition imposed by the wrapped event phase. Modeling the neutrino emission with an aperiodic Gaussian can cause a loss of statistical power, especially if the emission phase profile is wide and/or if the peak is close to the boundary. The parameters to be fitted in the temporal term are the phase peak, Φ_0, the concentration, κ which represents the spread of the events in phase, and the orbital period, P. A Gaussian prior centered at the measured period, $P_{\rm exp}$ is added to the likelihood ratio to facilitate the optimization of P (see Appendix A.1).

In addition to the initial source list discussed at the beginning of this section, binary sources from the 8 yr Fermi-LAT 4FGL gamma-ray catalog (Abdollahi et al. 2020) are also included in this analysis. Due to the limited sensitivity of IceCube to neutrino-induced track events in the Southern Sky, only sources with a decl. greater than −5° are selected. Since the focus is on sources with known periodicity, the next step excludes sources without a measured period, leaving 55 sources.

Results—No evidence for periodic neutrino emission is found. The most significant source is V635 Cas, which is an HMXB consisting of a Be star and a NS. The pre-trial significance is 2.6σ, which results in a post-trial p-value of 0.25. The distribution of signal-like events is shown in the top panel of Figure 1 as a function of the phase. The full results are tabulated in Appendix B.

3.2. Flare Analysis

This analysis focuses on searching for a correlation between the neutrino emission and the X-ray activity of a source. Hard X-ray light curves are used to construct the time PDF. Light curves are obtained from data reported by Swift/BAT 15–50 keV band[65] (Krimm et al. 2013) and MAXI 10–20 keV band[66] (Matsuoka et al. 2009). The X-ray light curves are binned in days, and a Bayesian block algorithm is applied to find the optimal segmentation of the data and identify flares (Scargle et al. 2013). After the light curves are divided into blocks, the flux data points inside each segment can be fitted as a constant value taking into account the uncertainty of the X-ray data. The normalized blocked light curves over the total livetime then act as the time PDF, mimicking the assumed neutrino flaring. Time-related parameters introduced here are the threshold of the X-ray flux $f_{\rm th}$ which removes irrelevant variation thus picks flares, and the potential time lag L_t between the X-ray and the neutrino emission. A more detailed description can be found in Appendix A.2.

Starting from our initial source list, sources without available Swift/BAT or MAXI hard X-ray light curves are removed. Furthermore, the variability and excess variance (see Appendix A.2) of the light curves are evaluated such that sources with weak or steady emission are also removed. This

[64] http://tevcat.uchicago.edu

[65] https://swift.gsfc.nasa.gov/results/transients/index.html

[66] http://maxi.riken.jp/top/slist.html

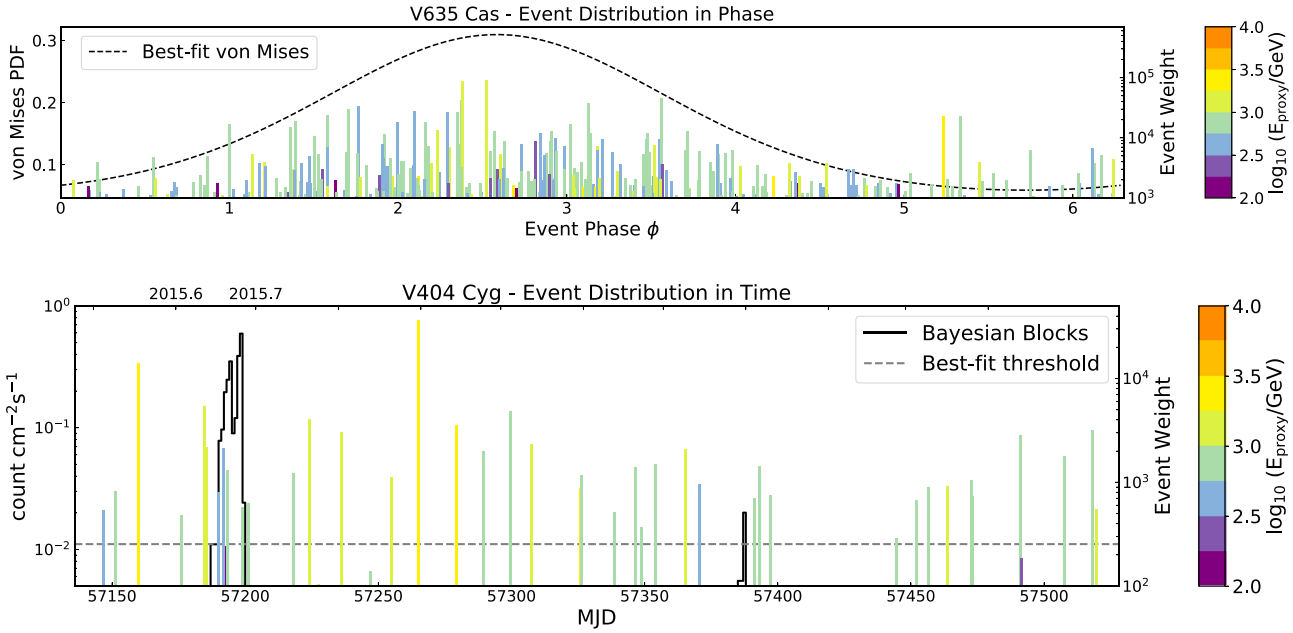

Figure 1. Top: The time PDF and the event distribution within a 10° zenith band centered at V635 Cas covering the whole 7.5 yr data set with the time converted to the phase ϕ according to the best-fit parameters. Vertical lines represent neutrino events. The color shows the energy proxy while the height shows the weight of each event in the likelihood function, assuming an E^{-2} spectrum. Bottom: The time PDF before normalization (Bayesian blocks) and the event distribution within 1.5° around V404 Cyg in the data sample of 2015 at the time indicated by MJD. The major X-ray flare happened in the 2015 June. The Bayesian blocks have been shifted by the best-fit time lag and the dashed gray line indicates the best-fit threshold. The vertical lines are read the same way as in the top panel.

step is applied only to the X-ray data in the time frame overlapped by the neutrino data sample. As neutrino emission is more likely to be correlated with harder X-ray emission, which is more probable to be nonthermal, the Swift/BAT light curves are selected over MAXI light curves cases where both pass the selection criteria. After this selection, there are 102 sources from the initial source list left to be analyzed.

Results—No significant signal events are found in the flare analysis, and results of all sources in this analysis can be found in Appendix B. The most significant source in the flare analysis is the microquasar V404 Cyg, a low-mass BH XRB, with a post-trial p-value of 0.75. There are five sub-TeV neutrino events within 1.5° of the source at the time of the major X-ray flare in 2015, and the best-fit threshold indicates a time duration of 11 days, as seen in the bottom panel of Figure 1. This giant X-ray flare was observed with a duration of approximately 13 days by Swift/BAT.[67]

3.3. Time-integrated Analysis

To complement the time-dependent studies, we conduct a time-integrated search for neutrinos on four notable sources: Cyg X-3, LS 5039, LS I+61 303, and SS 433. These are sources widely discussed as potential CR accelerators (see e.g., Gaisser & Stanev 1985; Aharonian et al. 2006; Christiansen et al. 2006; Torres & Halzen 2007; Reynoso & Carulli 2019; Kimura et al. 2020). Time-integrated tests on these four sources use the method described in Braun et al. (2008).

Results—In the time-integrated analysis, we did not find any significant signal. The most significant excess is found for Cyg X-3, which exhibits a post-trial p-value 0.036 after considering the 4 trials in the time-integrated analysis. Within 1° around the source location, there are 44 events, and the most energetic among them has a deposited energy about 5 TeV, leading to a soft best-fit power-law spectrum ($\gamma = 3.25$).

4. Discussion

In the absence of any significant signal, 90% confidence level (C.L.) upper limits (ULs) are computed for the sources with assumed spectra, which are shown in Appendix B. There is an overlap of 30 sources between the periodic and flare analyses. V635 Cas, the source with the smallest p-value in the periodic analysis, shows clear flaring episodes in the Swift/BAT light curves, which yields a pre-trial p-value of 0.16 in the flare analysis. The most significant source in the flare analysis V404 Cyg has a pre-trial p-value of 0.92 in the periodic analysis. In both periodic and flaring analyses, Cyg X-3 is one of the top 10 sources. On the whole, all results are consistent with the null hypothesis.

For non-microquasar XRBs with an NS as the compact object such as V635 Cas, the most significant source in the periodic study, it is possible that the CRs are accelerated in the magnetosphere, and neutrinos can be produced via CR interactions with the accretion disk through pp interactions. A similar scenario has been studied in detail for A 0535+26, an HMXB with an accreting neutron star, suggesting possible periodic neutrino emission by Anchordoqui et al. (2003). The flux prediction and the UL derived from the periodic analysis are shown in Figure 2. The UL is calculated for a power-law spectrum with a cutoff at 1 TeV. The current UL is comparable to the predicted flux, yet not enough to impose a constraint on the predicted neutrino flux from the model. The range of the estimated sensitivity with 15 yr of IceCube data due to varying the duty cycle is also shown in Figure 2, and it suggests that this model could likely be constrained by a future IceCube analysis with an extended livetime.

[67] https://www.astronomerstelegram.org/?read=7755

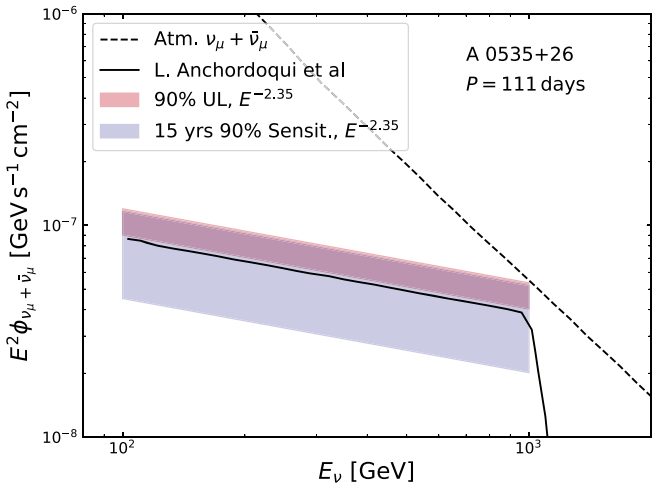

Figure 2. The neutrino flux prediction made by Anchordoqui et al. (2003) is shown as the black line. The black dashed line is the conventional atmospheric $\nu_\mu + \bar{\nu}_\mu$ flux integrated over a solid angle of IceCube's typical angular uncertainty. This flux is calculated using the H3a CR model (Gaisser 2012) and the SIBYLL2.3 c hadronic interaction model (Fedynitch et al. 2019). The range of the UL derived from the periodic analysis under different phase concentrations is shown as the pink band. The estimated sensitivity for a periodic analysis with 15 yr of IceCube data is shown as the purple band.

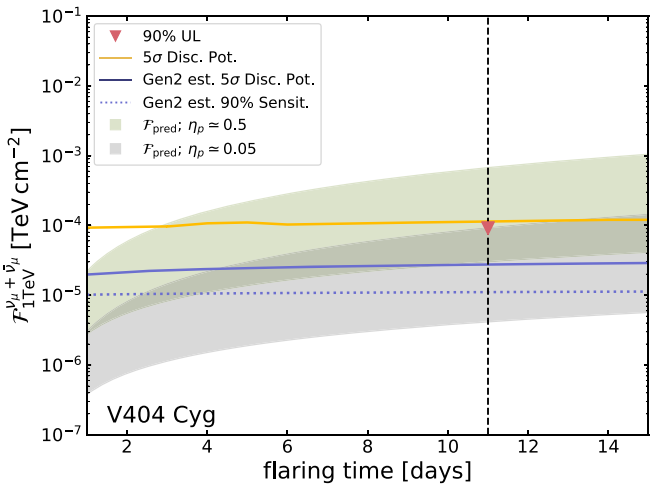

Figure 3. The relation between the fluence at 1 TeV and the flaring time for V404 Cyg. The vertical dashed black line is the flaring time converted from the best-fit threshold, and the red triangle shows the 90% C.L. UL in the flare search. The orange line is the 5σ discovery potential in IceCube. Purple lines illustrate the estimated sensitivity (dotted) at 90% C.L. and 5σ discovery potential (solid) in IceCube-Gen2. The shaded regions are the time-integrated neutrino flux prediction estimated following the jet model (Distefano et al. 2002), assuming an E^{-2} spectrum with an energy cutoff at 100 TeV. The two colors correspond to different energy fractions of the jet carried by accelerated protons η_p. The uncertainties are from flux densities in different frequencies in Very Large Array (VLA) radio measurements (Tetarenko et al. 2019) during the 2015 flare.

The most significant source in the flare search, V404 Cyg, is a microquasar. For microquasars, relativistic jets are expected to be CR acceleration sites. Possible neutrino emission is expected from the beam dump on either radiation from the compact object itself or gas from the companion star. Here, we employ the parameters for neutrino flux prediction in Distefano et al. (2002), based on the photohadronic model of Levinson & Waxman (2001). The flare of V404 Cyg in 2015 June was observed in a multi-wavelength campaign, and the jet activity during that outburst was studied, e.g., in Miller-Jones et al. (2019), Tetarenko et al. (2019). A simple estimation of the neutrino flux using the jet model can be performed with the radio jet information when the source is in an outburst state. The comparison between the ULs and the predicted fluence is shown in Figure 3. The CR interaction region in the source is estimated from the flaring duration, and the spectrum is assumed to follow a power-law distribution ($\gamma = 2$) with an exponential cutoff at 100 TeV, motivated by spectrum of Fermi acceleration and maximal expected Galactic CR energies. Regarding jet models, the magnetic energy and the kinetic energy in the jets are usually assumed to be in equipartition, leading to large magnetic fields, which may imply a strong attenuation of pions and muons at high energies, decreasing the neutrino flux compared to the simple calculations (Reynoso & Romero 2009). An alternative scenario considers neutrino emission through jet-wind interactions further away from the jet base (Reynoso & Romero 2009).

Cyg X-3, the most significant source in the time-integrated search, is one of the microquasars identified as a gamma-ray source early in observations. Many predictions have been calculated in the past decades assuming different models for high-energy emission from microquasars (see e.g., Gaisser & Stanev 1985; Kolb et al. 1985; Berezinskii et al. 1986; Bednarek 2005). For comparison, we take Baerwald & Guetta (2013) and Sahakyan et al. (2014), which discussed the general $p\gamma$ and pp scenarios. It is important to mention that Cyg X-3 lies in the direction of the Cygnus X region and is close to the Cygnus OB2 association, which is potentially one of the PeV point sources detected by LHAASO (Cao et al. 2021). Source contamination from the Cygnus X complex cannot be excluded.

For TeV XRBs, in a recent ANTARES time-integrated point-source search (Illuminati 2021), HESS J0632+057 has a pre-trial p-value 0.02 while this periodic analysis finds a pre-trial p-value 9.0×10^{-3}, the second most significant in the analysis. However, the flare search gives a pre-trial p-value of 1 while it is not included in the time-integrated search. Nevertheless, the hadronic component of the TeV gamma-ray observation cannot be constrained, and the significance is not large enough for any conclusion. For SS 433, more years of observation are needed to constrain the hadronic fraction of the observed TeV emission by HAWC (Abeysekara et al. 2018) and flux prediction in e.g., Kimura et al. (2020) while prediction in Distefano et al. (2002) is strongly constrained. More data are also needed to constrain LS 5039, which lies in the Southern Sky, and LS I +61 303, where the neutrino flux calculation from e.g., Torres & Halzen (2007) is not constrained by the upper limit. For the discussion above, the absorption of gamma-rays in the source is not considered. This is a notable effect if the production happens in the inner jet where there are dense target photons, to which we can expect a higher emitted high-energy gamma-ray flux than the measured one (Dubus 2006; Reynoso et al. 2008; Cerutti et al. 2011). For SS 433, our upper limit is at the same level as the most optimistic scenario in Reynoso & Carulli (2019).

The next generation of the IceCube Observatory, IceCube-Gen2, will provide a factor of eight extension in volume (Aartsen et al. 2020b), leading to an expected five-fold increase in the effective area compared to IceCube, corresponding to an improvement in sensitivity by the same order. Here, we extend the study to IceCube-Gen2 and estimate

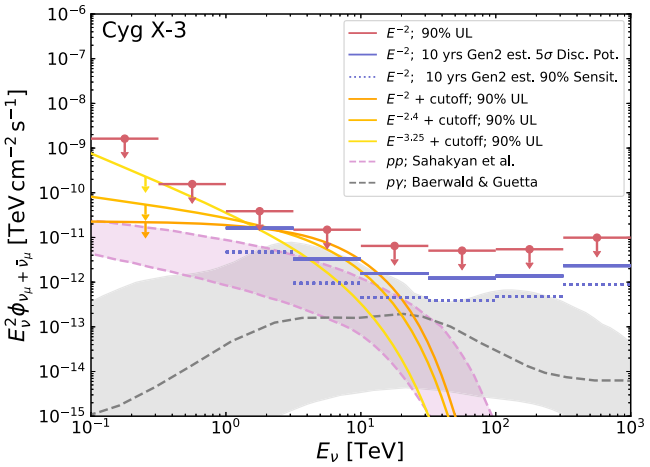

Figure 4. Red and purple lines indicate a comparison between current UL and estimated 10 yr sensitivity (dotted) and discovery potential (solid) in IceCube-Gen2. As the nearby events cut at several TeV, an exponential cutoff at 5 TeV is also applied for computing ULs. The shaded regions show predictions of pp and $p\gamma$ scenarios. The inclusion of a cutoff is also to be compared to the shaded pink region, which includes a cutoff of CR energy at 100 TeV with the spectral index ranging from 2.4 to 2.7. The gray shaded region shows the uncertainty from the collision radius.

the sensitivity and discovery potential for V404 Cyg, as an example of a flaring source and Cyg X-3, for persistently emitting sources. The estimated improvement can be seen in Figures 3 and 4. Here, the effective areas of muon tracks are computed from the proposed IceCube-Gen2 configuration, and the projection is evaluated with the same method as in Aartsen et al. (2020b) without considering contribution from the existing IceCube detector. In comparison with theoretical calculations, it demonstrates the potential to either identify those sources or better constrain models in the future. Therefore, providing a better estimation of the hadronic component of TeV gamma-ray sources.

5. Conclusion and Outlook

In this paper, we presented a comprehensive study on neutrino emission from XRBs, a long-standing candidate for the Galactic sources of CRs and neutrinos. With no significant signal events found, we set ULs on the neutrino emission in the scenarios presented with a discussion. Our estimation with the improved sensitivity of IceCube-Gen2 demonstrates the potential of future detection, presenting a promising outlook of identifying XRBs as Galactic cosmic-ray accelerators in the upcoming years.

The IceCube collaboration acknowledges the significant contributions to this manuscript from Ali Kheirandish, Qinrui Liu and Chun Fai Tung. The authors gratefully acknowledge the support from the following agencies and institutions: USA —U.S. National Science Foundation-Office of Polar Programs, U.S. National Science Foundation-Physics Division, U.S. National Science Foundation-EPSCoR, Wisconsin Alumni Research Foundation, Center for High Throughput Computing (CHTC) at the University of Wisconsin—Madison, Open Science Grid (OSG), Extreme Science and Engineering Discovery Environment (XSEDE), Frontera computing project at the Texas Advanced Computing Center, U.S. Department of Energy-National Energy Research Scientific Computing Center, Particle astrophysics research computing center at the University of Maryland, Institute for Cyber-Enabled Research at Michigan State University, and Astroparticle physics computational facility at Marquette University; Belgium—Funds for Scientific Research (FRS-FNRS and FWO), FWO Odysseus and Big Science programmes, and Belgian Federal Science Policy Office (Belspo); Germany—Bundesministerium für Bildung und Forschung (BMBF), Deutsche Forschungsgemeinschaft (DFG), Helmholtz Alliance for Astroparticle Physics (HAP), Initiative and Networking Fund of the Helmholtz Association, Deutsches Elektronen Synchrotron (DESY), and High Performance Computing cluster of the RWTH Aachen; Sweden—Swedish Research Council, Swedish Polar Research Secretariat, Swedish National Infrastructure for Computing (SNIC), and Knut and Alice Wallenberg Foundation; Australia—Australian Research Council; Canada —Natural Sciences and Engineering Research Council of Canada, Calcul Québec, Compute Ontario, Canada Foundation for Innovation, WestGrid, and Compute Canada; Denmark—Villum Fonden and Carlsberg Foundation; New Zealand—Marsden Fund; Japan—Japan Society for Promotion of Science (JSPS) and Institute for Global Prominent Research (IGPR) of Chiba University; Korea—National Research Foundation of Korea (NRF); Switzerland—Swiss National Science Foundation (SNSF); United Kingdom—Department of Physics, University of Oxford.

Appendix A
Method

The general form of the likelihood in this work can be written as

$$\mathcal{L} = \prod_i^N \left[\frac{n_s}{N} \mathcal{S}_i + \left(1 - \frac{n_s}{N}\right) \mathcal{B}_i \right], \tag{A1}$$

where i indicates the ith event, n_s is the number of signal events, N is the total number of events, and $\mathcal{S}_i$, $\mathcal{B}_i$ are the signal and background PDFs evaluated for event i, respectively. The signal PDF is the product of three terms,

$$\mathcal{S}_i = \mathcal{P}(x_i, \sigma_i | x_s) \times \mathcal{E}(E_i|\gamma) \times \mathcal{T}(t_i|\theta_1, \theta_2 ...), \tag{A2}$$

where $\mathcal{P}$, $\mathcal{E}$ and $\mathcal{T}$ are the PDFs of space, energy and time, respectively. x_i is the reconstructed incoming direction, σ_i is the estimated angular uncertainty, E_i is the reconstructed muon energy, and t_i is the arrival time of the event. The spatial clustering of signal events, represented by $\mathcal{P}$, can be modeled as a 2D Gaussian distribution; the energy term $\mathcal{E}$ is modeled by a simple power-law spectrum with spectral index γ, and the detector response is determined by the Monte Carlo simulation. In this work, the fitting range of γ is set to 1–4. For a time-integrated search, the time term $\mathcal{T}$ corresponds to a uniform distribution, in search for a steady emission of neutrinos. For sources with flaring or periodic characteristics, signal events can cluster in small timescales. Inclusion of a time selection can reduce the background effectively, thus improve the sensitivity (Braun et al. 2010). The background PDF $\mathcal{B}_i = 1/(2\pi)\mathcal{P}_B(\delta_i) \times \mathcal{E}_B(E_i)$ is constructed by binning the experimental data in reconstructed decl. and energy, based on the assumption that background events dominate the data. It is independent of the R.A. due to the Earth's rotation. The time distribution of the

background is assumed to be uniform, considering that the effect of seasonal variation is negligible.

A.1. Periodic Search

The signal time PDF is expressed as a phase PDF modeled by the von Mises distribution

$$\mathcal{T}(t_i|\kappa, \Phi_0, P) = \frac{1}{2\pi I_0(\kappa)} \times \exp\left[\kappa \cos\left(\phi_i(t_i|P) - \Phi_0\right)\right], \quad \text{(A3)}$$

where ϕ_i is the phase of the event which is a function of the arrival time, t_i and the orbital period, P of the source using the equation $\phi_i = (t_i - T_0)/P$, with T_0 set to MJD 55690. The value T_0 is chosen to reduce the error accumulated by the possible uncertainty in P. κ measures the concentration of events within a period, and Φ_0 is the mean phase of the distribution. κ, Φ_0, P, along with n_s and γ, are free parameters.

The TS in this analysis is

$$TS = -2\log\left[\frac{\mathcal{L}(n_s = 0)}{\mathcal{L}(\hat{n}_s, \hat{\gamma}, \hat{\kappa}, \hat{\Phi}_0, \hat{P})} \times \frac{2\pi}{\sigma_\Psi(\hat{\kappa})}\right] - 2\frac{(\hat{P} - P_{\rm exp})^2}{2\sigma_P^2}. \quad \text{(A4)}$$

Similar to the previous time-dependent analysis by Aartsen et al. (2015), the likelihood ratio is modified by a marginalization term $2\pi/\sigma_\Psi(\hat{\kappa})$ to prevent the minimizer from showing biases toward short flares, where σ_Ψ is the standard deviation of the von Mises distribution given by

$$\sigma_\Psi(\kappa) = \sqrt{-2\log\left(\frac{I_1(\kappa)}{I_0(\kappa)}\right)}. \quad \text{(A5)}$$

The second term is the prior probability of the orbital period of the source. It is approximated by a normal distribution centered at the measured orbital period P_{exp}, and the variance σ_P^2 is chosen as the reported uncertainty of $P_{\rm exp}$. The role of the prior is to facilitate the minimization of the orbital period with the information provided by the electromagnetic observations of the sources.

A.2. Flare Search

The method is similar to the IceCube triggered flare search in Aartsen et al. (2015). The Bayesian block algorithm is applied to the daily binned X-ray data to characterize statistically significant variations, thus remove noise and identify flares. The signal time PDF is constructed from the Bayesian blocked X-ray light curve and can be written as

$$\mathcal{T}(t_i|f_{\rm th}, t_{\rm lag}) = \frac{max(0,\ f(t_i - t_{\rm lag}) - f_{\rm th})}{\int_{T_{\rm min}}^{T_{\rm max}} max(0,\ f(t_i - t_{\rm lag}) - f_{\rm th})dt}, \quad \text{(A6)}$$

where f is the count rate of the light curve, which is a function of time and $f_{\rm th}$ is the count rate threshold. Only the light curve above the threshold is kept, which picks out the flares we care about while the irrelevant variation below the threshold is removed. $t_{\rm lag}$ is the time lag, which accounts for the time difference between X-ray flares and neutrino flares. This time lag comes from two factors: the first is the time difference between X-ray and neutrino emissions, which is not expected to be a large value; the second is the uncertainty of binning, as X-ray light curves used in this analysis are daily binned and the real emission time is unknown. We allow a uniform time lag prior of ± 0.5 days for fitting. The TS is defined as the maximal log-likelihood ratio $\mathrm{TS} = -2\log[(\mathcal{L}(n_s = 0)/\mathcal{L}(\hat{n}_s, \hat{\gamma}, \hat{f}_{\rm th}, \hat{t}_{\rm lag})]$.

The source selection is based on the variability which describes how variable the data is, and the excess variance which identifies flares of X-ray light curves (Krimm et al. 2013)

$$V_X = \frac{1}{N_X - 1}\sum_i^{N_X} \frac{(F_{{\rm X},i} - F_{\rm X,avg})^2}{\sigma_{{\rm X},i}}$$
$$F_{\rm X,var} = \frac{1}{F_{\rm X,avg}}\sqrt{\frac{\sum(F_{{\rm X},i} - F_{\rm X,avg})^2}{N_X - 1} - \frac{\sum\sigma_{{\rm X},i}^2}{N_X}}, \quad \text{(A7)}$$

where $F_{{\rm X},i}$ is the individual measurement of a source flux, $F_{\rm X,avg}$ is the weighted average and $N_{\rm X}$ is the total number of measurements. $\sigma_{{\rm X},i}$ includes both statistical and systematic errors.

Appendix B
Source Tables

The initial source list includes 301 X-ray binary sources from the HMXB and LMXB catalogs. On top of those, 7 binary sources from the TeVCat, which are not listed in the previous two, are added to the initial list. In the periodic search, 31 sources from the HMXB, 22 from the LMXB, and 1 from TeVCat HESS J0632+057, which have resolved orbital periods and declinations above -5° are selected. An extra source, 3FGL J0212.1+5320 from the 4FGL catalog, is added to form the analysis source list of 55 sources. In the flare search, there are 43 HMXB and 58 LMXB from the catalogs covering the whole sky with one extra HMXB HESS J0632+057 from TeVCat, which compose the total 102 sources after the selection. There are 30 sources overlapping in the two analyses. The full results of the periodic, flare, and time-integrated analyses are tabulated in Table 2, 3, and 4, respectively.

Table 2
Sources and Results of the Periodic Search

Source	R.A. (deg)	δ (deg)	TS	$\hat{n}_s$	$\hat{\gamma}$	$\hat{\kappa}$	$\hat{\Phi}_0$	$\hat{P}$	p-value	$\Phi^{90\%,\,E^{-2.0}}_{\nu_\mu+\bar{\nu}_\mu}$	$\Phi^{90\%,\,E^{-3.0}}_{\nu_\mu+\bar{\nu}_\mu}$
V1037 Cas	7.26	59.57	−2.63	0.0	3.92	0.5	1.63	0.102	0.76	0.74	8.17
BD +60 73	9.29	61.36	−2.36	6.9	4	0.5	5.8	15.66	0.51	0.71	8.3
4U 0042+32	11.21	33.02	2.56	17.5	4	21.1	4.12	11.588	0.22	0.77	16.1
gam Cas	14.18	60.72	−1.79	13.4	4	0.5	1.68	203.59	0.41	0.78	9.11
V662 Cas	19.51	65.29	0.1	25.8	4	1.79	4.02	11.599	0.22	1.29	14.2
V635 Cas	19.63	63.74	9.07	50.5	4	0.83	2.58	24.316	0.0052	2.67	28.5
3FGL J0212.1+5320	33.04	53.35	1.04	19.8	3.01	0.5	3.38	0.869	0.19	1.08	14.6
LS I+61 303	40.13	61.23	−2.63	0.0	3.54	0.5	2.18	26.496	0.86	0.71	7.99
BQ Cam	53.75	53.17	0.108	17.4	3.3	10.2	1.34	33.85	0.17	0.93	14.6
X Per	58.85	31.05	−1.17	15.6	3.89	2.26	4.63	250.3	0.31	0.62	11.4
CI Cam	64.93	56.00	−2.63	0.0	3.99	0.5	4.99	19.41	0.89	0.72	7.74
V518 Per	65.43	32.91	−2.16	9.4	3.48	0.5	2.54	0.212	0.48	0.55	8.18
LS V+44 17	70.25	44.53	−2.63	0.0	3.14	0.5	1.78	150	0.90	0.55	7.75
1A 0535+262	84.73	26.32	−2.63	0.0	3.96	0.5	0.08	111	0.70	0.47	8.93
Swift J061223.0+701243.9	93.09	70.21	−0.439	1.6	1.19	0.5	0.84	0.013	0.32	1.34	13.6
V1055 Ori	94.28	9.14	4.75	17.8	2.65	59.6	6.18	0.028	0.099	0.69	25.5
V616 Mon	95.69	−0.35	0.523	27.5	3.71	1.26	4.7	0.323	0.20	0.44	18.9
HESS J0632+057	98.25	5.80	11.3	39.7	3.73	23.6	0.75	308.75	0.0090	0.78	38.5
SAX J0635.2+0533	98.83	5.55	0.308	18.8	2.93	10.1	0.48	11.168	0.36	0.38	14.7
KV UMa	169.55	48.04	−2.23	1.6	1.99	0.5	3	0.170	0.51	0.58	7.86
UW CrB	241.44	25.86	−1.39	17.8	4	0.5	5.92	0.077	0.34	0.63	12.2
Her X-1	254.46	35.34	−0.718	20.1	4	0.5	2.08	1.700	0.26	0.75	12.1
V934 Her	256.64	23.97	−2.63	1.2	3.98	0.5	1.24	420.17	0.72	0.40	7.8
Swift J1753.5-0127	268.37	−1.45	−2.63	0.0	2.61	0.5	2.74	0.135	0.73	0.25	9.95
4U 1823-00	276.34	−0.01	3.87	22.7	3.38	18.6	5.35	0.133	0.16	0.43	23.6
AX 1845.0-0433	281.26	−4.56	2.42	30.6	3.93	0.5	5.15	5.720	0.056	0.69	35
IGR J18483-0311	282.07	−3.18	−2.63	0.0	3.16	0.5	1.32	18.545	0.65	0.27	11.1
2S 1845-024	282.07	−2.42	−2.63	0.0	2.76	0.5	4.81	242.18	0.95	0.24	11.4
XTE J1855-026	283.88	−2.61	−2.54	4.7	3.72	0.5	4.34	6.074	0.53	0.28	10.8
V406 Vul	284.67	22.66	1.26	23.9	3.34	5.06	0.89	0.274	0.27	0.60	14.6
XTE J1859+083	284.77	8.25	−2.63	0.0	2.16	0.5	4.29	60.65	0.87	0.31	9.75
4U 1901+03	285.90	3.19	−2.63	0.0	3.46	0.5	4.65	22.535	0.67	0.28	10.8
4U 1907+09	287.41	9.83	2.7	37.6	4	0.5	2.97	8.375	0.060	0.69	24.7
4U 1909+07	287.70	7.60	0.14	29.0	4	0.5	4.93	4.400	0.18	0.58	17.6
Aql X-1	287.82	0.58	−2.53	2.0	2.48	0.5	4.6	0.790	0.64	0.26	9.9
SS 433	287.96	4.98	−2.63	0.0	2.76	0.5	3.26	13.068	0.84	0.25	9.95
IGR J19140+0951	288.52	9.88	−0.162	24.6	4	6.27	2.99	13.553	0.20	0.47	16.9
GRS 1915+105	288.80	10.95	−0.865	23.4	3.77	0.5	2.78	33.862	0.31	0.52	15
XTE J1946+274	296.41	27.37	5.61	35.8	3.52	2.87	5.58	171.1	0.026	0.11	24.7
KS 1947+300	297.38	30.21	−2.63	0.0	3.03	0.5	1.32	40.415	0.91	0.47	8.29
Cyg X-1	299.59	35.20	−2.63	0.0	1.25	0.5	0.39	5.600	0.83	0.50	7.89
V1408 Aql	299.85	11.71	−2.63	0.0	2.77	0.5	1.34	0.389	0.91	0.34	8.92
QZ Vul	300.71	25.24	−2.63	0.0	2.64	0.5	5.01	0.344	0.78	0.48	8.38
V404 Cyg	306.02	33.87	−2.63	0.0	4	0.5	1.6	6.473	0.92	0.47	7.89
V2246 Cyg	308.06	37.64	−0.213	1.5	1.17	0.5	3.06	46.021	0.19	0.84	13.2
Cyg X-3	308.11	40.95	7.46	50.6	3.52	1.06	4.82	0.200	0.045	1.38	22.9
GRO J2058+42	314.70	41.78	−2.63	0.0	3.88	0.5	0.65	55.03	0.79	0.51	7.54
SAX J2103.5+4545	315.90	45.75	−2.46	4.0	2.55	0.5	1.7	12.665	0.52	0.53	7.9
M15 X-2	322.49	12.17	−2.37	8.2	3.8	0.5	6.27	0.016	0.56	0.35	10
M15 X-1	322.49	12.17	−2.59	3.5	3.99	0.5	3.01	0.713	0.64	0.30	9.43
V1727 Cyg	322.86	47.29	0.452	17.4	4	8.35	0.15	0.218	0.16	0.91	14.7
V490 Cep	324.88	56.99	−0.477	1.5	1	1.33	5.31	20.848	0.32	0.90	12
Cyg X-2	326.17	38.32	−0.0499	20.6	4	0.5	5.95	9.845	0.20	0.90	13.3
BD +53 2790	331.98	54.52	−0.275	16.3	4	1.98	1.02	9.56	0.21	1.07	12.8
SAX J2239.3+6116	339.84	61.27	3.09	23.5	4	12.1	0.6	265.62	0.088	1.22	16.4

Note. Sources for the periodic point-source analysis with their best-fitted TS, $\hat{n}_s$, $\hat{\gamma}$, $\hat{\kappa}$, $\hat{\Phi}_0$, P (in days), and pre-trial p-values. The 90% C.L. flux ULs are parameterized as $dN_{\nu_\mu+\bar{\nu}_\mu}/dE_\nu = \Phi^{90\%,\,E^{-\gamma}}_{\nu_\mu+\bar{\nu}}(E_\nu/\mathrm{TeV})^{-\gamma}$ where γ indicates the assumed spectral index of a power-law spectrum, and their units are $10^{-12}\,\mathrm{TeV}^{-1}\,\mathrm{cm}^{-2}\,\mathrm{s}^{-1}$. The equatorial coordinates are provided in the J2000 epoch, which also applies to other tables in this paper.

Table 3
Sources and Results of the Flare Search

Source	R.A. (deg)	δ (deg)	TS	$\hat{n}_s$	$\hat{\gamma}$	$\hat{f}_{\rm th}$	$\hat{T}_{\rm lag}$	p-value	$\mathcal{F}^{90\%,\,E^{-2.0}}_{\nu_\mu+\bar{\nu}_\mu}$	$\mathcal{F}^{90\%,\,E^{-2.5}}_{\nu_\mu+\bar{\nu}_\mu}$	$\mathcal{F}^{90\%,\,E^{-3.0}}_{\nu_\mu+\bar{\nu}_\mu}$
V662 Cas	19.51	65.29	1.54	14.8	4	0.03	−0.16	0.54	0.15	0.5	1.1
V635 Cas	19.63	63.74	2.69	2.3	2.46	8.23	−0.46	0.16	0.11	0.3	0.5
RX J0146.9+6121	26.75	61.36	0	0	…	…	…	1	0.30	0.3	2.6
BQ Cam	53.75	53.17	2.25	2.9	2.96	18.55	−0.25	0.16	0.09	0.4	0.6
X Per	58.85	31.05	2.62	17.2	3.60	0.60	0.49	0.37	0.07	0.4	0.9
LS V+44 17	70.25	44.53	1.53	1.9	4	0.58	−0.03	0.24	0.07	0.2	0.5
1A 0535+262	84.73	26.32	0	0	…	…	…	1	0.15	0.2	1.6
V1055 Ori	94.28	9.14	1.75	11.7	2.56	0.00	0.42	0.42	0.09	0.7	1.9
HESS J0632+057	98.25	5.80	0	0	…	…	…	1	0.14	0.3	3.1
GS 0834-430	128.98	−43.19	0	0	…	…	…	1	1.97	22.3	1536.4
Vela X-1	135.53	−40.55	2.22	2.8	4	6.73	0.35	0.41	0.95	33.9	704.2
GRO J1008-57	152.45	−58.29	0	0	…	…	…	1	3.76	38.2	3021.9
Cen X-3	170.31	−60.62	4.86	1.1	1.00	2.49	−0.05	0.18	1.83	78.3	1647.4
1E 1145.1-6141	176.87	−61.95	7.54	10.4	2.33	0.18	0.11	0.05	2.65	107.1	2295.8
GX 301-2	186.66	−62.77	2.43	1.8	2.49	18.91	−0.44	0.33	0.93	32.7	708.5
1A 1246-588	192.40	−59.12	0.20	0.5	2.00	4.47 [m]	−0.00	0.63	0.72	26.1	512.3
GX 304-1	195.32	−61.60	0.07	0.3	2.87	1.57	−0.16	0.47	0.97	32.8	612.0
4U 1323-619	201.65	−62.14	1.57	0.8	4	5.36 [m]	−0.50	0.38	0.80	26.6	520.8
Ginga 1354-645	209.54	−64.73	0	0	…	…	…	1	3.13	35.3	2371.7
H 1417-624	215.30	−62.70	0.13	0.5	1.60	0.12	−0.31	0.40	0.94	32.0	755.9
Cir X-1	230.17	−57.17	3.59	1.0	1.64	1.12	0.50	0.13	1.10	34.5	761.4
H 1538-522	235.60	−52.39	3.35	2.1	4	0.68	0.50	0.22	1.26	40.0	899.5
H 1553-542	239.45	−54.41	0	0	…	…	…	1	2.74	29.3	2325.7
H 1608-522	243.18	−52.42	0.13	0.4	4	1.23	0.50	0.59	0.71	27.5	532.0
Sco X-1	244.98	−15.64	3.86	6.8	4	29.05	0.33	0.18	0.40	12.6	202.0
IGR J16318-4848	247.95	−48.82	5.75	5.4	3.59	0.42	0.38	0.12	1.69	65.2	1476.7
AX J1631.9-4752	248.01	−47.87	2.87	0.9	1.75	1.80	0.47	0.34	0.60	18.5	386.0
4U 1630-472	248.51	−47.39	0	0	…	…	…	1	2.49	24.7	2214.6
4U 1636-536	250.23	−53.75	0	0	…	…	…	1	5.96	63.8	5666.3
GX 340+0	251.45	−45.61	0.54	1.5	3.13	1.67	−0.18	0.69	0.69	21.1	467.1
IGR J16479-4514	252.03	−45.20	6.11	2.7	2.35	0.96	−0.38	0.08	0.90	31.7	665.5
Her X-1	254.46	35.34	0	0	…	…	…	1	0.41	0.6	5.9
EXO 1657-419	255.20	−41.66	8.44	2.1	3.10	6.70	−0.50	0.02	1.05	33.2	690.8
GX 339-4	255.71	−48.79	0.22	0.8	1.96	2.67	0.47	0.54	0.67	24.5	497.3
4U 1700-377	255.99	−37.84	0.08	0.5	4	2.75	0.50	0.82	0.93	35.6	782.2
GX 349+2	256.44	−36.42	0.10	1.3	2.44	1.65	−0.41	0.86	0.69	25.9	667.4
4U 1702-429	256.56	−43.04	0	0	…	…	…	1	4.36	45.6	4569.1
4U 1700+24	256.64	23.97	3.38	6.5	4	0.48	0.44	0.23	0.07	0.4	0.8
H 1705-440	257.23	−44.10	4.60	6.6	4	0.48	0.13	0.09	1.61	62.5	1404.4
IGR J17091-3624	257.26	−36.39	1.35	3.0	2.31	0.32	−0.50	0.30	0.78	24.3	520.7
Granat 1716-249	259.90	−25.02	1.24	2.1	2.97	11.05	−0.21	0.34	0.38	12.7	227.6
IGR J17252-3616	261.30	−36.28	0.34	0.5	1.14	0.57	−0.48	0.69	0.46	15.9	307.4
4U 1722-30	261.89	−30.80	0	0	…	…	…	1	2.58	23.5	2184.6
GX 9+9	262.93	−16.96	6.62	1.0	2.24	20.27 [m]	−0.47	0.06	0.35	8.3	111.4
GX 354-0	262.99	−33.83	0	0	…	…	…	1	3.23	34.7	3641.9
GX 1+4	263.01	−24.75	0.13	0.5	3.38	2.52	−0.50	0.71	0.38	11.8	240.5
Rapid Burster	263.35	−33.39	0	0	…	…	…	1	2.40	21.6	2043.3
SLX 1732-304	263.95	−30.48	3.43	7.9	3.87	0.00 [m]	0.25	0.17	0.92	34.9	675.3
4U 1735-44	264.74	−44.45	0	0	…	…	…	1	4.00	36.6	3838.4
IGR J17391-3021	264.80	−30.34	0.75	0.8	2.53	0.07	−0.47	0.32	0.41	13.0	231.8
GRS 1739-278	265.67	−27.75	0	0	…	…	…	1	1.43	12.6	1131.0
1E 1740.7-2942	265.98	−29.75	0	0	…	…	…	1	3.05	33.9	2977.0
GRO J1744-28	266.14	−28.74	0.02	0.2	2.30	0.54	0.34	0.51	0.44	14.1	249.3
AX J1744.8-2921	266.21	−29.35	0	0	…	…	…	1	2.38	21.7	2297.1
Granat J1741.9-2853	266.26	−28.91	0	0	…	…	…	1	1.45	12.1	836.0
AX J1745.6-2901	266.42	−29.01	1.50	1.1	2.29	1.92	−0.50	0.23	0.40	12.9	228.5
1A 1742-294	266.52	−29.51	0.69	2.0	2.47	5.69 [m]	−0.41	0.50	0.45	14.6	295.8
IGR J17464-3213	266.56	−32.23	0	0	…	…	…	1	2.35	22.3	1955.6
GX 3+1	266.98	−26.56	0	0	…	…	…	1	2.25	20.7	2237.7
EXO 1745-248	267.02	−24.78	0.33	0.6	4	0.04	0.50	0.39	0.37	10.4	197.5
H 1745-203	267.22	−20.36	0	0	…	…	…	1	0.79	6.8	448.7
AX J1749.1-2639	267.30	−26.64	0	0	…	…	…	1	1.21	13.2	1077.4
SAX J1750.8-2900	267.60	−29.04	1.84	2.5	4	0.18	−0.48	0.21	0.65	23.3	419.6
SWIFT J1753.5-0127	268.37	−1.45	0.84	2.5	4	1.64	−0.50	0.53	0.03	0.3	0.7

Table 3
(Continued)

Source	R.A. (deg)	δ (deg)	TS	$\hat{n}_s$	$\hat{\gamma}$	$\hat{f}_{\rm th}$	$\hat{T}_{\rm lag}$	p-value	$\mathcal{F}^{90\%,\,E^{-2.0}}_{\nu_\mu+\bar{\nu}_\mu}$	$\mathcal{F}^{90\%,\,E^{-2.5}}_{\nu_\mu+\bar{\nu}_\mu}$	$\mathcal{F}^{90\%,\,E^{-3.0}}_{\nu_\mu+\bar{\nu}_\mu}$
SAX J1753.5-2349	268.39	−23.82	0	0	⋯	⋯	⋯	1	1.00	8.9	593.0
4U 1755-338	269.67	−33.81	0	0	⋯	⋯	⋯	1	1.41	15.7	1227.5
GX 5-1	270.28	−25.08	1.61	1.2	3.29	3.49	−0.37	0.47	0.38	9.7	192.6
GRS 1758-258	270.30	−25.74	0	0	⋯	⋯	⋯	1	2.69	25.0	2536.6
GX 9+1	270.38	−20.53	3.85	1.3	1.51	11.75 [m]	−0.49	0.19	0.65	27.6	511.5
SAX J1806.5-2215	271.64	−22.25	0.70	1.6	2.95	0.35	0.50	0.45	0.37	11.3	201.7
XTE J1807-294	271.75	−29.41	2.81	3.8	1.87	0.45 [m]	−0.23	0.20	0.81	29.6	622.7
SAX J1808.4-3658	272.12	−36.98	0	0	⋯	⋯	⋯	1	1.89	17.8	1333.1
GX 13+1	273.63	−17.16	0.43	1.0	1.87	0.65	0.46	0.75	0.22	6.8	107.7
GX 17+2	274.01	−14.04	1.47	4.7	3.53	1.89	−0.18	0.55	0.21	6.8	105.0
SAX J1819.3-2525	274.84	−25.43	0	0	⋯	⋯	⋯	1	1.38	15.0	1143.2
H 1820-303	275.92	−30.36	0	0	⋯	⋯	⋯	1	3.40	29.6	3323.0
IGR J18245-2452	276.12	−24.85	0.08	0.3	3.92	0.45	−0.45	0.51	0.25	7.3	123.3
Ginga 1826-238	277.37	−23.80	2.85	6.2	3.51	1.32	0.19	0.21	0.66	27.1	472.6
2S 1845-024	282.07	−2.42	1.57	2.5	3.93	0.62	−0.30	0.42	0.03	0.2	0.5
IGR J18483-0311	282.07	−3.18	0.03	0.7	4	0.33	−0.48	0.85	0.04	0.3	0.8
XTE J1855-026	283.88	−2.61	3.71	3.8	4	0.48	−0.20	0.21	0.05	0.4	1.0
XTE J1858+034	284.65	3.44	0.96	1.5	4	0.65	0.28	0.45	0.03	0.1	0.3
XTE J1859+083	284.77	8.25	0.09	1.0	4	0.56	−0.43	0.56	0.04	0.2	0.6
HT 1900.1-2455	285.04	−24.92	0	0	⋯	⋯	⋯	1	2.24	19.1	2008.2
XTE J1908+094	287.22	9.38	6.11	1.8	4	1.50	−0.13	0.03	0.06	0.3	0.6
4U 1907+09	287.41	9.83	5.54	2.8	2.26	1.23	−0.40	0.14	0.05	0.2	0.6
Aql X-1	287.82	0.58	0	0	⋯	⋯	⋯	1	0.13	0.3	3.7
SS 433	287.96	4.98	1.15	8.7	2.71	0.16	−0.19	0.57	0.05	0.3	1.1
IGR J19140+0951	288.52	9.88	4.48	25.3	4	0.10	−0.23	0.24	0.09	0.6	1.6
GRS 1915+105	288.80	10.95	4.61	16.4	4	8.07	−0.42	0.19	0.09	0.7	1.9
4U 1916-053	289.70	−5.24	0	0	⋯	⋯	⋯	1	0.26	0.6	7.8
XTE J1946+274	296.41	27.37	3.21	5.8	2.50	0.00	0.00	0.09	0.10	0.5	1.0
KS 1947+300	297.38	30.21	0	0	⋯	⋯	⋯	1	0.24	0.3	3.0
4U 1954+31	298.93	32.10	0.08	4.0	4	0.00	0.25	0.83	0.08	0.4	0.9
Cyg X-1	299.59	35.20	4.68	4.0	2.81	22.43	−0.43	0.17	0.08	0.3	0.7
V404 Cyg	306.02	33.87	8.28	5.4	4	1.11	−0.50	0.01	0.09	0.4	0.8
V2246 Cyg	308.06	37.64	4.24	1.3	1.09	0.55	−0.04	0.14	0.16	0.8	1.7
Cyg X-3	308.11	40.95	8.36	21.4	4	4.61	0.34	0.09	0.19	0.9	2.2
SAX J2103.5+4545	315.90	45.75	2.15	6.6	1.97	0.00	−0.50	0.29	0.15	0.6	1.4
V490 Cep	324.88	56.99	0.05	0.4	2.69	0.29	0.11	0.61	0.07	0.2	0.5
Cyg X-2	326.17	38.32	2.44	17.9	4	0.48	0.21	0.42	0.14	0.7	2.2
BD +53 2790	331.98	54.52	1.15	10.3	4	0.00	−0.34	0.57	0.11	0.5	0.9

Note. Sources for the flare analysis with their best-fitted TS, $\hat{n}_s$, $\hat{\gamma}$, threshold $\hat{f}_{\rm th}$, time lag $\hat{T}_{\rm lag}$ and pre-trial p-values. The threshold has units 10^{-2} count cm^{-2} s^{-1} and the superscript [m] indicates the use of MAXI light curves while others use *Swift*/BAT light curves. The time lag is represented in days. The 90% C.L. fluence ULs are parameterized as $E^2 dN_{\nu_\mu+\bar{\nu}_\mu}/dE_\nu = \mathcal{F}^{90\%,\,E^{-\gamma}}_{\nu_\mu+\bar{\nu}_\mu}(E_\nu/\mathrm{TeV})^{-\gamma} \cdot 10^{-3}$ TeV cm^{-2}, where γ indicates the assumed spectral index of a power-law spectrum.

Table 4
Time-integrated Sources and Results

Source	R.A. (deg)	δ (deg)	TS	$\hat{n}_s$	$\hat{\gamma}$	p-value	$\Phi^{90\%,\,E^{-2.0}}_{\nu_\mu+\bar{\nu}_\mu}$	$\Phi^{90\%,\,E^{-2.5}}_{\nu_\mu+\bar{\nu}_\mu}$	$\Phi^{90\%,\,E^{-3.0}}_{\nu_\mu+\bar{\nu}_\mu}$
LSI +61 303	40.13	61.23	0	0	⋯	1	0.76	3.16	7.59
LS 5039	276.56	−14.85	0.62	5.78	3.62	0.382	1.45	50.43	834.94
SS 433	287.96	4.98	0	0	⋯	1	0.30	2.85	9.95
Cyg X-3	308.11	40.95	6.80	44.58	3.25	0.009	1.51	8.60	24.59

Note. Sources for the time-integrated analysis with their best-fitted TS, $\hat{n}_s$, $\hat{\gamma}$ and pre-trial p-values. The 90% C.L. flux UL are parameterized as $dN_{\nu_\mu+\bar{\nu}_\mu}/dE_\nu = \phi^{90\%,\,E^{-\gamma}}_{\nu_\mu+\bar{\nu}_\mu}(E_\nu/\mathrm{TeV})^{-\gamma} \cdot 10^{-12}$ TeV^{-1} cm^{-2} s^{-1}, where γ indicates the assumed spectral index of a power-law spectrum.

ORCID iDs

R. Abbasi https://orcid.org/0000-0001-6141-4205
M. Ackermann https://orcid.org/0000-0001-8952-588X
J. A. Aguilar https://orcid.org/0000-0003-2252-9514
M. Ahlers https://orcid.org/0000-0003-0709-5631
J. M. Alameddine https://orcid.org/0000-0002-9534-9189
G. Anton https://orcid.org/0000-0003-2039-4724
C. Argüelles https://orcid.org/0000-0003-4186-4182
Y. Ashida https://orcid.org/0000-0003-4136-2086
A. Balagopal V. https://orcid.org/0000-0001-5367-8876

S. W. Barwick https://orcid.org/0000-0003-2050-6714
V. Basu https://orcid.org/0000-0002-9528-2009
S. Baur https://orcid.org/0000-0002-3329-1276
J. J. Beatty https://orcid.org/0000-0003-0481-4952
J. Becker Tjus https://orcid.org/0000-0002-1748-7367
J. Beise https://orcid.org/0000-0002-7448-4189
C. Bellenghi https://orcid.org/0000-0001-8525-7515
S. BenZvi https://orcid.org/0000-0001-5537-4710
E. Bernardini https://orcid.org/0000-0003-3108-1141
D. Z. Besson https://orcid.org/0000-0001-6733-963X
E. Blaufuss https://orcid.org/0000-0001-5450-1757
S. Blot https://orcid.org/0000-0003-1089-3001
S. Böser https://orcid.org/0000-0002-5918-4890
O. Botner https://orcid.org/0000-0001-8588-7306
F. Bradascio https://orcid.org/0000-0002-7750-5256
A. Burgman https://orcid.org/0000-0003-1276-676X
M. A. Campana https://orcid.org/0000-0003-4162-5739
C. Chen https://orcid.org/0000-0002-8139-4106
D. Chirkin https://orcid.org/0000-0003-4911-1345
B. A. Clark https://orcid.org/0000-0003-4089-2245
K. Clark https://orcid.org/0000-0003-2467-6825
A. Coleman https://orcid.org/0000-0003-1510-1712
J. M. Conrad https://orcid.org/0000-0002-6393-0438
P. Coppin https://orcid.org/0000-0001-6869-1280
P. Correa https://orcid.org/0000-0002-1158-6735
D. F. Cowen https://orcid.org/0000-0003-4738-0787
R. Cross https://orcid.org/0000-0003-0081-8024
P. Dave https://orcid.org/0000-0002-3879-5115
C. De Clercq https://orcid.org/0000-0001-5266-7059
J. J. DeLaunay https://orcid.org/0000-0001-5229-1995
D. Delgado López https://orcid.org/0000-0002-4306-8828
H. Dembinski https://orcid.org/0000-0003-3337-3850
A. Desai https://orcid.org/0000-0001-7405-9994
P. Desiati https://orcid.org/0000-0001-9768-1858
K. D. de Vries https://orcid.org/0000-0002-9842-4068
G. de Wasseige https://orcid.org/0000-0002-1010-5100
T. DeYoung https://orcid.org/0000-0003-4873-3783
A. Diaz https://orcid.org/0000-0001-7206-8336
J. C. Díaz-Vélez https://orcid.org/0000-0002-0087-0693
H. Dujmovic https://orcid.org/0000-0003-1891-0718
M. A. DuVernois https://orcid.org/0000-0002-2987-9691
P. Eller https://orcid.org/0000-0001-6354-5209
P. A. Evenson https://orcid.org/0000-0001-7929-810X
A. R. Fazely https://orcid.org/0000-0002-6907-8020
A. Fedynitch https://orcid.org/0000-0003-2837-3477
C. Finley https://orcid.org/0000-0003-3350-390X
D. Fox https://orcid.org/0000-0002-3714-672X
A. Franckowiak https://orcid.org/0000-0002-5605-2219
P. Fürst https://orcid.org/0000-0002-7951-8042
T. K. Gaisser https://orcid.org/0000-0003-4717-6620
E. Ganster https://orcid.org/0000-0003-4393-6944
A. Garcia https://orcid.org/0000-0002-8186-2459
S. Garrappa https://orcid.org/0000-0003-2403-4582
A. Ghadimi https://orcid.org/0000-0002-6350-6485
C. Glaser https://orcid.org/0000-0001-5998-2553
T. Glauch https://orcid.org/0000-0003-1804-4055
T. Glüsenkamp https://orcid.org/0000-0002-2268-9297
S. Griswold https://orcid.org/0000-0002-7321-7513
P. Gutjahr https://orcid.org/0000-0001-7980-7285
A. Hallgren https://orcid.org/0000-0001-7751-4489
L. Halve https://orcid.org/0000-0003-2237-6714
F. Halzen https://orcid.org/0000-0001-6224-2417
A. Haungs https://orcid.org/0000-0002-9638-7574
D. Hebecker https://orcid.org/0000-0002-2643-7126
K. Helbing https://orcid.org/0000-0003-2072-4172
F. Henningsen https://orcid.org/0000-0002-0680-6588
C. Hill https://orcid.org/0000-0003-0647-9174
F. Huang https://orcid.org/0000-0002-6014-5928
M. Huber https://orcid.org/0000-0002-6515-1673
K. Hultqvist https://orcid.org/0000-0003-0602-9472
N. Iovine https://orcid.org/0000-0001-7965-2252
G. S. Japaridze https://orcid.org/0000-0002-7000-5291
M. Jin https://orcid.org/0000-0003-0487-5595
B. J. P. Jones https://orcid.org/0000-0003-3400-8986
D. Kang https://orcid.org/0000-0002-5149-9767
W. Kang https://orcid.org/0000-0003-3980-3778
A. Kappes https://orcid.org/0000-0003-1315-3711
T. Karg https://orcid.org/0000-0003-3251-2126
M. Karl https://orcid.org/0000-0003-2475-8951
A. Karle https://orcid.org/0000-0001-9889-5161
U. Katz https://orcid.org/0000-0002-7063-4418
M. Kauer https://orcid.org/0000-0003-1830-9076
J. L. Kelley https://orcid.org/0000-0002-0846-4542
A. Kheirandish https://orcid.org/0000-0001-7074-0539
S. R. Klein https://orcid.org/0000-0003-2841-6553
A. Kochocki https://orcid.org/0000-0003-3782-0128
R. Koirala https://orcid.org/0000-0002-7735-7169
H. Kolanoski https://orcid.org/0000-0003-0435-2524
L. Köpke https://orcid.org/0000-0001-8530-6348
C. Kopper https://orcid.org/0000-0001-6288-7637
D. J. Koskinen https://orcid.org/0000-0002-0514-5917
P. Koundal https://orcid.org/0000-0002-5917-5230
M. Kovacevich https://orcid.org/0000-0002-5019-5745
M. Kowalski https://orcid.org/0000-0001-8594-8666
N. Kurahashi https://orcid.org/0000-0003-1047-8094
C. Lagunas Gualda https://orcid.org/0000-0002-9040-7191
M. J. Larson https://orcid.org/0000-0002-6996-1155
F. Lauber https://orcid.org/0000-0001-5648-5930
J. P. Lazar https://orcid.org/0000-0003-0928-5025
K. Leonard https://orcid.org/0000-0002-8795-0601
A. Leszczyńska https://orcid.org/0000-0003-0935-6313
Q. R. Liu https://orcid.org/0000-0003-3379-6423
E. Lohfink https://orcid.org/0000-0003-3248-5682
L. Lu https://orcid.org/0000-0003-3175-7770
F. Lucarelli https://orcid.org/0000-0002-9558-8788
A. Ludwig https://orcid.org/0000-0001-9038-4375
W. Luszczak https://orcid.org/0000-0003-3085-0674
Y. Lyu https://orcid.org/0000-0002-2333-4383
W. Y. Ma https://orcid.org/0000-0003-1251-5493
J. Madsen https://orcid.org/0000-0003-2415-9959
K. B. M. Mahn https://orcid.org/0000-0002-5771-1124
R. Maruyama https://orcid.org/0000-0003-2794-512X
F. McNally https://orcid.org/0000-0002-0785-2244
K. Meagher https://orcid.org/0000-0003-3967-1533
S. Mechbal https://orcid.org/0000-0002-8579-3964
M. Meier https://orcid.org/0000-0002-9483-9450
S. Meighen-Berger https://orcid.org/0000-0001-6579-2000
T. Montaruli https://orcid.org/0000-0001-5014-2152
R. W. Moore https://orcid.org/0000-0003-4160-4700
M. Moulai https://orcid.org/0000-0001-7909-5812
R. Naab https://orcid.org/0000-0003-2512-466X
R. Nagai https://orcid.org/0000-0001-7503-2777
J. Necker https://orcid.org/0000-0003-0280-7484
H. Niederhausen https://orcid.org/0000-0002-9566-4904

M. U. Nisa https://orcid.org/0000-0002-6859-3944
A. Obertacke Pollmann https://orcid.org/0000-0002-2492-043X
B. Oeyen https://orcid.org/0000-0003-2940-3164
E. O'Sullivan https://orcid.org/0000-0003-1882-8802
H. Pandya https://orcid.org/0000-0002-6138-4808
N. Park https://orcid.org/0000-0002-4282-736X
E. N. Paudel https://orcid.org/0000-0001-9276-7994
C. Pérez de los Heros https://orcid.org/0000-0002-2084-5866
A. Pizzuto https://orcid.org/0000-0002-8466-8168
M. Plum https://orcid.org/0000-0001-8691-242X
A. Porcelli https://orcid.org/0000-0002-3220-6295
C. Raab https://orcid.org/0000-0001-9921-2668
M. Rameez https://orcid.org/0000-0001-5023-5631
A. Rehman https://orcid.org/0000-0001-7616-5790
R. Reimann https://orcid.org/0000-0002-1983-8271
E. Resconi https://orcid.org/0000-0003-0705-2770
S. Reusch https://orcid.org/0000-0002-7788-628X
W. Rhode https://orcid.org/0000-0003-2636-5000
B. Riedel https://orcid.org/0000-0002-9524-8943
M. Rongen https://orcid.org/0000-0002-7057-1007
C. Rott https://orcid.org/0000-0002-6958-6033
D. Ryckbosch https://orcid.org/0000-0002-8759-7553
D. Rysewyk Cantu https://orcid.org/0000-0002-3612-6129
I. Safa https://orcid.org/0000-0001-8737-6825
A. Sandrock https://orcid.org/0000-0002-6779-1172
M. Santander https://orcid.org/0000-0001-7297-8217
S. Sarkar https://orcid.org/0000-0002-3542-858X
S. Sarkar https://orcid.org/0000-0002-1206-4330
K. Satalecka https://orcid.org/0000-0002-7669-266X
A. Schneider https://orcid.org/0000-0002-0895-3477
J. Schneider https://orcid.org/0000-0001-7752-5700
F. G. Schröder https://orcid.org/0000-0001-8495-7210
S. Sclafani https://orcid.org/0000-0001-9446-1219
M. Silva https://orcid.org/0000-0001-6940-8184
B. Smithers https://orcid.org/0000-0003-1273-985X
J. Soedingrekso https://orcid.org/0000-0003-1011-2797
D. Soldin https://orcid.org/0000-0003-3005-7879
G. M. Spiczak https://orcid.org/0000-0002-0030-0519
C. Spiering https://orcid.org/0000-0001-7372-0074
J. Stachurska https://orcid.org/0000-0002-0238-5608
R. Stein https://orcid.org/0000-0003-2434-0387
J. Stettner https://orcid.org/0000-0003-1042-3675
T. Stezelberger https://orcid.org/0000-0003-2676-9574
T. Stuttard https://orcid.org/0000-0001-7944-279X
G. W. Sullivan https://orcid.org/0000-0002-2585-2352
I. Taboada https://orcid.org/0000-0003-3509-3457
S. Ter-Antonyan https://orcid.org/0000-0002-5788-1369
K. Tollefson https://orcid.org/0000-0001-9725-1479
S. Toscano https://orcid.org/0000-0002-1860-2240
A. Trettin https://orcid.org/0000-0003-0350-3597
C. F. Tung https://orcid.org/0000-0001-6920-7841
A. Turcati https://orcid.org/0000-0002-8050-7869
C. F. Turley https://orcid.org/0000-0002-9689-8075
M. A. Unland Elorrieta https://orcid.org/0000-0002-6124-3255
J. Vandenbroucke https://orcid.org/0000-0002-9867-6548
N. van Eijndhoven https://orcid.org/0000-0001-5558-3328
J. van Santen https://orcid.org/0000-0002-2412-9728
S. Verpoest https://orcid.org/0000-0002-3031-3206
C. Walck https://orcid.org/0000-0002-4188-9219
T. B. Watson https://orcid.org/0000-0002-8631-2253
C. Weaver https://orcid.org/0000-0003-2385-2559
J. Weldert https://orcid.org/0000-0002-3709-2354
C. Wendt https://orcid.org/0000-0001-8076-8877
N. Whitehorn https://orcid.org/0000-0002-3157-0407
C. H. Wiebusch https://orcid.org/0000-0002-6418-3008
M. Wolf https://orcid.org/0000-0001-9991-3923
S. Yoshida https://orcid.org/0000-0003-2480-5105
T. Yuan https://orcid.org/0000-0002-7041-5872

References

Aartsen, M. G., Abbasi, R., Abdou, Y., et al. 2013a, Sci, 342, 1242856
Aartsen, M. G., Abbasi, R., Abdou, Y., et al. 2013b, ApJ, 779, 132
Aartsen, M. G., Ackermann, M., Adams, J., et al. 2014, PhRvL, 113, 101101
Aartsen, M. G., Ackermann, M., Adams, J., et al. 2015, ApJ, 807, 46
Aartsen, M. G., Ackermann, M., Adams, J., et al. 2017a, ApJ, 849, 67
Aartsen, M. G., Ackermann, M., Adams, J., et al. 2017b, JInst, 12, P03012
Aartsen, M. G., Ackermann, M., Adams, J., et al. 2017c, APh, 92, 30
Aartsen, M. G., Ackermann, M., Adams, J., et al. 2018a, Sci, 361, 147
Aartsen, M. G., Ackermann, M., Adams, J., et al. 2018b, Sci, 361, eaat1378
Aartsen, M. G., Ackermann, M., Adams, J., et al. 2020a, ApJ, 898, 117
Aartsen, M. G., Abbasi, R., Ackermann, M., et al. 2021, JPhG, 48, 060501
Abbasi, R., Abdou, Y., Abu-Zayyad, T., et al. 2012, ApJ, 748, 118
Abdollahi, S., Acero, F., Ackermann, M., et al. 2020, ApJS, 247, 33
Abeysekara, A. U., Albert, A., Alfaro, R., et al. 2018, Natur, 562, 82
Adrian-Martinez, S., Albert, A., André, M., et al. 2014, JHEAp, 3, 9
Aharonian, F., & Atoyan, A. 1991, ApJ, 381, 220
Aharonian, F. A., Anchordoqui, L. A., Khangulyan, D., & Montaruli, T. 2006, JPhCS, 39, 408
Albert, A., André, M., Anton, G., et al. 2017, JCAP, 04, 019
Albert, A., André, M., Anghinolfi, M., et al. 2018, ApJL, 868, L20
Anchordoqui, L. A., Torres, D. F., McCauley, T. P., Romero, G. E., & Aharonian, F. A. 2003, ApJ, 589, 481
Baerwald, P., & Guetta, D. 2013, ApJ, 773, 159
Bednarek, W. 2005, ApJ, 631, 466
Berezinskii, V., Castagnoli, C., & Galeotti, P. 1986, ApJ, 301, 235
Berezinsky, V. S., Castagnoli, C., & Galeotti, P. 1985, NCimC, 8, 185
Braun, J., Baker, M., Dumm, J., et al. 2010, APh, 33, 175
Braun, J., Dumm, J., De Palma, F., et al. 2008, APh, 29, 299
Cao, Z., Aharonian, F., An, Q., et al. 2021, Natur, 594, 33
Cerutti, B., Dubus, G., Malzac, J., et al. 2011, A&A, 529, A120
Cheng, K., & Ruderman, M. 1989, ApJL, 337, L77
Christiansen, H. R., Orellana, M., & Romero, G. E. 2006, PhRvD, 73, 063012
Distefano, C., Guetta, D., Waxman, E., & Levinson, A. 2002, ApJ, 575, 378
Dubus, G. 2006, A&A, 451, 9
Fedynitch, A., Riehn, F., Engel, R., Gaisser, T. K., & Stanev, T. 2019, PhRvD, 100, 103018
Gaisser, T. K. 2012, APh, 35, 801
Gaisser, T. K., & Stanev, T. 1985, PhRvL, 54, 2265
Illuminati, G. 2021, ICRC (Berlin), 395, 1161
Kheirandish, A., & Wood, J. 2020, ICRC (Madison, WI), 36, 932
Kimura, S. S., Murase, K., & Mészáros, P. 2020, ApJ, 904, 188
Kolb, E. W., Turner, M. S., & Walker, T. P. 1985, PhRvD, 32, 1145
Krimm, H. A., Holland, S. T., Corbet, R. H. D., et al. 2013, ApJS, 209, 14
Levinson, A., & Waxman, E. 2001, PhRvL, 87, 171101
Liu, Q. Z., van Paradijs, J., & Heuvel, E. P. J. V. D. 2006, A&A, 455, 1165
Liu, Q. Z., van Paradijs, J., & Heuvel, E. P. J. V. D. 2007, A&A, 469, 807
Matsuoka, M., Kawasaki, K., Ueno, S., et al. 2009, PASJ, 61, 999
Miller-Jones, J. C. A., Tetarenko, A. J., Sivakoff, G. R., et al. 2019, Natur, 569, 374
Mirabel, I., Rodriguez, L., Cordier, B., Paul, J., & Lebrun, F. 1992, Natur, 358, 215
Reynoso, M. M., & Carulli, A. M. 2019, APh, 109, 25
Reynoso, M. M., Christiansen, H. R., & Romero, G. E. 2008, APh, 28, 565
Reynoso, M. M., & Romero, G. E. 2009, A&A, 493, 1
Romero, G. E., Torres, D. F., Bernado, M. M. K., & Mirabel, I. F. 2003, A&A, 410, L1
Romero, G. E., & Vila, G. S. 2008, A&A, 485, 623
Sahakyan, N., Piano, G., & Tavani, M. 2014, ApJ, 780, 29
Scargle, J. D., Norris, J. P., Jackson, B., & Chiang, J. 2013, ApJ, 764, 167
Tetarenko, A. J., Sivakoff, G. R., Miller-Jones, J. C. A., et al. 2019, MNRAS, 482, 2950
Torres, D. F., & Halzen, F. 2007, APh, 27, 500
Wakely, S. P., & Horan, D. 2008, ICRC (Mérida), 3, 1341